ISSN 1674-1056
http://cpb.iphy.ac.cn
http://iopscience.iop.org/cpb
中国物理 B
Chinese Physics
中国物理 Chinese Physics B

Review on non-dipole effects in ionization and harmonic generation of atoms and molecules

Mu-Xue Wang(王慕雪)[1], Si-Ge Chen(陈思格)[1], Hao Liang(梁昊)[1], Liang-You Peng(彭良友)[1,2,3,4]

Citation: Chin. Phys. B . 2020, 29(1): 013302 . **doi:** 10.1088/1674-1056/ab5c10
Journal homepage: http://cpb.iphy.ac.cn; http://iopscience.iop.org/cpb

What follows is a list of articles you may be interested in

Observation of the optical $X^2\Sigma_g^+$-$A^2\Pi_u$ coupling in N_2^+ lasing induced by intense laser field

Siqi Wang(王思琪), Yao Fu(付尧), Danwen Yao(姚丹雯), Shanming Chen(陈善铭), Wei Zhang(张维), Helong Li(李贺龙), Huailiang Xu(徐淮良)

Chin. Phys. B . 2019, 28(12): 123301 . **doi:** 10.1088/1674-1056/ab54b1

Attosecond transient absorption spectroscopy: Comparative study based on three-level modeling

Zeng-Qiang Yang(杨增强), Di-Fa Ye(叶地发), Li-Bin Fu(傅立斌)

Chin. Phys. B . 2018, 27(1): 013301 . **doi:** 10.1088/1674-1056/27/1/013301

Photoelectron longitudinal momentum distributions containing nondipole effects

Yi-Ning Huo(霍一宁), Jian Li(李健), Feng-Cai Ma(马凤才)

Chin. Phys. B . 2018, 27(1): 013203 . **doi:** 10.1088/1674-1056/27/1/013203

Frequency dependence of quantum path interference in non-collinear high-order harmonic generation

Shi-Yang Zhong(钟诗阳), Xin-Kui He(贺新奎), Hao Teng(滕浩), Peng Ye(叶蓬), Li-Feng Wang(汪礼锋), Peng He(何鹏), Zhi-Yi Wei(魏志义)

Chin. Phys. B . 2016, 25(2): 023301 . **doi:** 10.1088/1674-1056/25/2/023301

Quantum path control using attosecond pulse trains via UV-assisted resonance enhance ionization

Li Fang, Wei Lai, He Zhi-Cong

Chin. Phys. B . 2015, 24(4): 043301 . **doi:** 10.1088/1674-1056/24/4/043301

TOPICAL REVIEW — Strong field atomic and molecular physics

Review on non-dipole effects in ionization and harmonic generation of atoms and molecules*

Mu-Xue Wang(王慕雪)[1], Si-Ge Chen(陈思格)[1], Hao Liang(梁昊)[1], and Liang-You Peng(彭良友)[1,2,3,4,†]

[1] State Key Laboratory for Artificial Microstructure and Mesoscopic Physics, School of Physics, Peking University, Beijing 100871, China
[2] Nano-optoelectronics Frontier Center of the Ministry of Education and Collaborative Innovation Center of Quantum Matter, Beijing 100871, China
[3] Collaborative Innovation Center of Extreme Optics, Shanxi University, Taiyuan 030006, China
[4] Beijing Academy of Quantum Information Sciences, Beijing 100193, China

(Received 23 September 2019; revised manuscript received 22 November 2019; accepted manuscript online 27 November 2019)

In this review, we will focus on recent progress on the investigations of nondipole effects in few-electron atoms and molecules interacting with light fields. We first briefly survey several popular theoretical methods and relevant concepts in strong field and attosecond physics beyond the dipole approximation. Physical phenomena stemming from the breakdown of the dipole approximation are then discussed in various topics, including the radiation pressure and photon-momentum transfer, the atomic stabilization, the dynamic interference, and the high-order harmonic generation. Whenever available, the corresponding experimental observations of these nondipole effects are also introduced respectively in each topics.

Keywords: nondipole effects, photon-momentum, strong field approximation, attosecond physics

PACS: 33.20.Xx, 32.80.Rm, 42.65.Re **DOI:** 10.1088/1674-1056/ab5c10

1. Introduction

In most cases, the dipole approximation is used to simplify the theoretical treatment of the laser–matter interaction. The spatial dependence of the electromagnetic field of light is thus neglected and so one drops all higher orders of multipole interactions than the dipole one. This approximation is valid when the electromagnetic field has a wavelength much larger than the scale of the atomic and molecular system, which means that there is an upper limit on the light frequency to apply the dipole approximation.[1,2] In the short-wavelength regime, free-electron lasers (FELs)[3–5] can now produce x-rays at wavelengths down to 1 Å with an unprecedented intensity around 10^{20} W/cm^2 (see, *e.g.*, Ref. [6] and references therein). There also exists a lower limit to the frequency at which one can neglect the magnetic force of light.[7] In particular, recent advances in intense ultrafast lasers in the long wavelength regime,[8–14] has extended the strong-field sciences into mid-infrared (mid-IR) regime.[15–19] Technical developments in these new light sources have opened the door to experimentally investigate highly non-perturbative and relativistic effects in the laser–matter interaction. For the theoretical studies, the dipole approximation become invalid and nondipole effects can arise when the laser wavelength is comparable with the size of atoms or when the laser intensity increases so drastically that the electric and magnetic components of lights become equally important in the exhibition of the relativistic effects.[20,21]

The breakdown of the dipole approximation is expected to lead to a forward/backward asymmetry in the photoelectron angular distribution (PAD). For decades, a large number of researches have concentrated on experimentally measuring or theoretically calculating the nondipolar asymmetry parameters. Since the year around 1930, deviations from the dipole predictions have been shown in PADs for hard x-ray pulses with photon-energy well above 5 keV,[22–26] see also Ref. [27] and the references therein. Experimental[25,28–38] and theoretical[39–47] investigations on the nondipole effects in the PADs for the soft x-ray pulses with photon-energy below 5 keV can be traced back to the year of 1969. Nondipole effects have been observed at extremely low energies,[48–58] in which situations the dipole transition amplitude is usually depressed around a Cooper minimum[59] while the nondipole effect is resonance-enhanced. Measurements and calculations for the nondipole parameter of molecules have also been carried out, with a few debates on N_2.[60–71] We note that, recent measurements have been made on the angular emission distributions of the 1s-photoelectrons of N_2 ionized by linearly polarized synchrotron radiation at photon energy of 40 keV, in which an unexpected asymmetry with respect to the polarization direction has been observed.[72] Photoionization cross sections beyond the dipole approximation have been calculated for atoms through the full field operator,[73,74] which has also been used in Refs. [64,75] for molecules.

By integrating over those asymmetric electron distribu-

*Project supported by the National Natural Science Foundation of China (Grant Nos. 11961131008, 11725416, and 11574010) and the National Key Research and Development Program of China (Grant No. 2018YFA0306302).

†Corresponding author. E-mail: liangyou.peng@pku.edu.cn

© 2020 Chinese Physical Society and IOP Publishing Ltd

tions, one can obtain a net momentum of photoelectron along the direction of the light propagation, which comes from the linear photon-momentum partition between the photoelectrons and the residual ion. The photon-momentum transfer, which has been investigated respectively in the perturbative regime,[76–81] and in the tunneling regime,[77,79,82–95] can be used to measure the radiation pressure and give insights into the breakdown of the dipole approximation.

For the laser pulse at a high frequency and a super-high intensity, effects such as the atomic stabilization[96–108] and the dynamic interference,[109–120] which has been theoretically observed for decades, are in prospect of being demonstrated experimentally. The stabilization effect is expected to occur in a laser pulse at super-high intensities with its photon energy usually exceeding the binding potential of the system. In the case of atomic hydrogen, the stabilization can happen for photon energies above 13.6 eV and intensities higher than 10^{16} W/cm^2.[102,119,121,122] Calculations[123,124] show that the manifestation of the nondipole effect on the atomic stabilization relies on the pulse duration, in which a window of intermediate pulse durations where the atomic stabilization is enhanced by the nondipole terms was proposed. In particular, the magnetic component of the laser field shows a detrimental effect on the atomic stabilization for short external pulses.[122] For atomic hydrogen, the atomic stabilization is feasible for an external laser pulse at a moderately high frequency ($\sim$ 50 eV) and an extremely high intensity (above 10^{18} W/cm^2), thus making the dynamic interference possible.[119] In such a high-intensity laser field, dynamic interference patterns beyond the dipole approximation have been theoretically studied.[120]

In the long-wavelength limit, the magnetic field-induced drift of the photoelectron in the laser propagation direction may reduce the chance of the ionized electron to revisit the residual ion,[125–128] which is expected to weaken the rescattering and recombination process. This will lead to nondipole effects on the high-order above-threshold ionization (ATI)[129,130] and the high-order harmonic generation (HHG)[131–137] spectra, which in the latter case shows a decrease in the yield of photons emitted along the laser polarization direction.[138–145] Besides, the symmetry of the system under the dipole approximation will be broken due to the magnetic field, with the presence of even harmonics[146–148] and with photons emitted along the laser propagation direction.[140,144,149,150] Both of them are forbidden in the dipole approximation because of the parity and symmetry of the system.

With the consideration of the magnetic component of the light field, attention should be also paid to the electronic spin dynamics. The spin–magnetic coupling is in the order of $O(\alpha)$ and the spin–orbit coupling is in the order of $O(\alpha^2)$. Though comparable with the leading order of the nondipole terms, which includes the electric quadrupole and the magnetic dipole, the spin–magnetic coupling is negligible due to its spatial independence in the model with the lowest-order corrections beyond the dipole approximation. If higher-order multipole effects are considered, the spin–magnetic coupling becomes spatially dependent and the spin–orbit coupling is comparable with the second-order nondipole terms. Therefore, both of them need to be included in theoretical models and the electronic spin may play an important role in higher-order nondipole effects.[151–155] In practice, one needs to numerically solve the Dirac equation, instead of solving the time-dependent Schrödinger equation beyond the dipole approximation.

The rest of this review is arranged as follows. In Section 2, we will give a brief introduction to several popular numerical methods dealing with light–matter interaction beyond the dipole approximation. Then, the theoretical and experimental results are surveyed in the perturbative regime in Section 3 and in the non-perturbative regime with intense laser fields in Section 4. We will discuss the nondipole effects exhibiting in the PAD, the photon momentum transfer, the dynamic interference, and the HHG. Emphases are put on the cases of the few-electron atoms and molecules. A short conclusion and outlook will be drawn at last in Section 5. Note that atomic units (a.u.) will be used throughout unless otherwise stated.

2. Theoretical concepts and numerical methods

To describe the laser–matter interaction, an appropriate gauge form is crucial to the numerical convergence[156] and to the physical interpretation of the numerical results.[85] In the radiation gauge, the time-dependent Hamiltonian of a single-electron system interacting with a laser field is given by

$$H = \frac{1}{2}[\boldsymbol{p} + \boldsymbol{A}(\boldsymbol{r},t)]^2 + V(\boldsymbol{r}), \tag{1}$$

where $\boldsymbol{A}(\boldsymbol{r},t)$ is the vector potential of the light field and $V(\boldsymbol{r})$ is the Columbic potential between the electron and the nuclei. According to the plane wave approximation of the light field, the spatial and temporal distribution of the vector potential can be denoted by

$$\boldsymbol{A}(\boldsymbol{r},t) = \boldsymbol{A}(\tau), \tag{2}$$

in which the retarded time τ is given by $t - \alpha\hat{\boldsymbol{k}}\cdot\boldsymbol{r}$ with the unit vector $\hat{\boldsymbol{k}}$ being the laser propagation direction and α being the fine-structure constant. We can expand Eq. (2) in terms of α as

$$\boldsymbol{A}(\tau) = \boldsymbol{A}_0(t) + \alpha(\hat{\boldsymbol{k}}\cdot\boldsymbol{r})\boldsymbol{E}_0(t) + O(\alpha^2), \tag{3}$$

where $\boldsymbol{A}_0(t)$ and $\boldsymbol{E}_0(t)$ respectively represents the vector potential and the electric field at $\boldsymbol{r} = 0$. Inserting Eq. (3) into

Eq. (1), we can get

$$H = \frac{p^2}{2} + \boldsymbol{p}\cdot\boldsymbol{A}_0(t) + V(\boldsymbol{r}) + \alpha(\hat{\boldsymbol{k}}\cdot\boldsymbol{r}) \times [\boldsymbol{p}\cdot\boldsymbol{E}_0(t) + \boldsymbol{A}_0(t)\cdot\boldsymbol{E}_0(t)] + O(\alpha^2) \quad (4)$$

with $\alpha = 1/c$. In this review, only the leading-order nondipole terms of $O(\alpha)$ are taken into account, which correspond to the lowest-order nondipole effects in various processes.

The Hamiltonian in Eq. (4) has been widely used in numerical investigations of the nondipole effects.[77,80,89,91,157,158] Through gauge transformations, many other nondipole gauge forms and their corresponding Hamiltonian can be obtained.[122,159–161] For example, the Kramers–Henneberger frame resulting from the unitary Kramers–Henneberger's transformation is popular in the high-frequency regime.[122,162] By choosing the Powers–Zienau–Wolley gauge transformation,[163,164] the Hamiltonian in the multipolar gauge has been derived, in which the terms of the electric dipole, the electric quadrupole, and the magnetic dipole can be separated and explicitly expressed.[165] Anzaki *et al.*[166] provided a systematic investigation on the gauge invariance to all orders of non-dipole correlations in various gauges. Such a formulation is convenient for separately investigating how the inhomogeneity of electric field and magnetic field will affect the electron dynamics in light fields.

To solve the time-dependent Schrödinger equation corresponding to the Hamiltonian (4) or its equivalent variants, one can adopt different methods, depending on the specific problems in different regimes. In the rest of this section, we will briefly survey these methods. The basic quantity to be computed is the differential distribution of the photoelectrons or the harmonics. The other physical observable can be further evaluated.

2.1. Time-dependent perturbation method

For a light field at a relatively weak intensity, the lowest-order perturbation theory (LOPT) can be applied to the one-photon ionization process. Deriving from the Hamiltonian in Eq. (4), the expression of the one-photon transition amplitude from the initial bound state $\Psi_i(\boldsymbol{r})\mathrm{e}^{\mathrm{i}I_p t}$ to a final continuum state $\Psi_{\boldsymbol{p}}^{(-)}(\boldsymbol{r})\mathrm{e}^{-\mathrm{i}E_p t}$ is[167]

$$A_1(\boldsymbol{p}) = (-\mathrm{i})\langle\Psi_{\boldsymbol{p}}^{(-)}|\boldsymbol{p}\cdot\hat{\boldsymbol{A}}(E_p - E_\mathrm{i}) + \alpha(\hat{\boldsymbol{k}}\cdot\boldsymbol{r})\boldsymbol{p}\cdot\hat{\boldsymbol{E}}_0(E_p - E_\mathrm{i})|\Psi_i\rangle.$$

Likewise, the second-order perturbation theory can be used in the two-photon ionization process.[168,169] In the formulation of the Green's function, the two-photon transition amplitude beyond the dipole approximation can be shown to be[81]

$$A_2(\boldsymbol{p}) = \langle\Psi_{\boldsymbol{p}}^{(-)}| - \frac{1}{2\pi}\int \mathrm{d}\varepsilon[\boldsymbol{p}\cdot\hat{\boldsymbol{A}}(E_p - \varepsilon) + \alpha(\hat{\boldsymbol{k}}\cdot\boldsymbol{r})\boldsymbol{p}\cdot\hat{\boldsymbol{E}}(E_p - \varepsilon)]G_\varepsilon(\boldsymbol{r},\boldsymbol{r}') \times [\boldsymbol{p}\cdot\hat{\boldsymbol{A}}(\varepsilon - E_\mathrm{i}) + \alpha(\hat{\boldsymbol{k}}\cdot\boldsymbol{r}')\boldsymbol{p}\cdot\hat{\boldsymbol{E}}(\varepsilon - E_\mathrm{i})] + \alpha(\hat{\boldsymbol{k}}\cdot\boldsymbol{r})\hat{F}(E_p - E_\mathrm{i})|\Psi_i\rangle, \quad (5)$$

where $E_\mathrm{i} = -I_p$ is the initial state energy and $E_p = p^2/2$ is the final kinetic energy of the electron with momentum $\boldsymbol{p} = (p, \hat{\boldsymbol{p}}) = (p, \theta, \phi)$. Note that $\hat{\boldsymbol{A}}(\omega) = \int_{t_0}^{t_\mathrm{f}} \boldsymbol{A}_0(t)\mathrm{e}^{\mathrm{i}\omega t}\mathrm{d}t$ is the Fourier transform of $\boldsymbol{A}_0(t)$ and $\hat{\boldsymbol{E}}(\omega)$ is the Fourier transform of $\boldsymbol{E}_0(t)$. The function $\hat{F}(E_p - E_\mathrm{i})$ is defined to be

$$\hat{F}(E_p - E_\mathrm{i}) = \int_{t_0}^{t_\mathrm{f}} \boldsymbol{A}_0(t)\cdot\boldsymbol{E}_0(t)\mathrm{e}^{\mathrm{i}(E_p - E_\mathrm{i})t}\mathrm{d}t. \quad (6)$$

In Eq. (5), the Coulomb–Green's function (CGF) for the atomic hydrogen[170–172]

$$G_\varepsilon(\boldsymbol{r},\boldsymbol{r}') = \sum_{klm}\frac{|\Psi_{klm}\rangle\langle\Psi_{klm}|}{E_k - \varepsilon} + \int \mathrm{d}\boldsymbol{p}\frac{|\Psi_{\boldsymbol{p}}^{(-)}\rangle\langle\Psi_{\boldsymbol{p}}^{(-)}|}{p^2/2 - \varepsilon - \mathrm{i}0} \quad (7)$$

can be expanded through the spherical harmonics, *i.e.*,

$$G_\varepsilon(\boldsymbol{r},\boldsymbol{r}') = \sum_{lm} g_l(\varepsilon;\boldsymbol{r},\boldsymbol{r}')\mathrm{Y}_{lm}(\hat{\boldsymbol{r}})\mathrm{Y}_{lm}^*(\hat{\boldsymbol{r}}'). \quad (8)$$

The radial part $g_l(\varepsilon;\boldsymbol{r},\boldsymbol{r}')$ can be developed into series in Sturm's function of the Coulomb problem and the result can rapidly converge for a negative value of the virtual intermediate state's energy ε.[172]

With the above formulations, the three-dimensional photoelectron momentum distribution (PMD) can be obtained by $P(\boldsymbol{p}) = |A_1(\boldsymbol{p})|^2$ and $P(\boldsymbol{p}) = |A_2(\boldsymbol{p})|^2$ for the one- and two-photon ionizations.

2.2. Semi-classical description

Non-perturbative phenomena can occur when the laser intensity is sufficiently strong, which is beyond the description of the perturbation theory. In the case of intense infrared (IR) or mid-IR pulses, the electron dynamics can be treated semi-classically in the combined force of the electromagnetic field and the Coulomb potential. For example, the classical trajectory Monte Carlo (CTMC) simulations[173,174] is widely used to interpret the experimental data and to analyze the Coulomb effects in atomic ionization. In the CTMC model, the probability $W(t_i, v_\perp)$ of an electron released from the atomic bound state at the moment t_i and with an initial transverse velocity $v_\perp$ is weighted by the PPT[175] ionization rate (or the ADK[176] ionization rate in the adiabatic picture). The tunneling electron is assumed to have a Gaussian transverse (perpendicular to the instantaneous electric field) velocity distribution,

$$W'(v_\perp) \propto \left[\sqrt{2I_p}/|\boldsymbol{E}(t_i)|\right]\exp\left[-\sqrt{2I_p}(v_\perp)^2/|\boldsymbol{E}(t_i)|\right], \quad (9)$$

in which $v_\perp$ is the electron initial transverse velocity. The longitudinal velocity parallel to the instantaneous electric field at the ionization moment is normally taken to be zero. The initial position of the electron is at the tunnel exit, where it is released from the ion.

After sampling the initial conditions of all electrons, their classical motion is governed by the Newton's equation until the external field is turned off. With the leading-order ($O(\alpha)$) nondipole term included, the motion equation of electrons ionized from the hydrogen atom in the combined electromagnetic field and the Coulomb field is

$$\ddot{\boldsymbol{r}} = -\boldsymbol{E} - \boldsymbol{v}\times\boldsymbol{B} - \boldsymbol{r}/r^3, \tag{10}$$

where r is the distance from the electron to the nucleus and the magnetic field is given by

$$\boldsymbol{B} = \alpha\hat{\boldsymbol{k}}\times\boldsymbol{E}. \tag{11}$$

After the end of the laser pulse, the electron with a positive energy is regarded as ionized, and its final momentum is given by the Kepler's formula. Finally, the electrons appearing at the tunnel exit at the time t_i and with a similar final momentum $\boldsymbol{p}$ will be put into a bin. The ionization probability is the sum of all electrons' weight in the bin,

$$P(\boldsymbol{p}) = \sum_j W_j, \tag{12}$$

where j means the j-th electron in the bin and $W_j \propto \left[(2I_p)^2/|\boldsymbol{E}(t_i)|\right]^{2/\sqrt{2I_p}-1}\exp\left[-2(2I_p)^{1.5}/3|\boldsymbol{E}(t_i)|\right]W'(v_\perp^j)$.

The above CTMC model beyond the dipole approximation have been applied to investigate the nondipole effects, such as the transfer and the partition of the photon linear momentum in atomic ionization.[84,93,177,178]

2.3. Strong field approximation

Besides the aforementioned semiclassical description, one can also develop a quantum mechanical formulation by generalizing the usual strong field approximation to the nondipole case. Applying an analytical expression of the nondipole Volkov state[79] and keeping the leading-order nondipole term, one can arrive at the transition amplitude from the initial bound state to the final state

$$M_{\boldsymbol{p}} = -\mathrm{i}\int_{t_0}^{t_f}\mathrm{d}\tau\left[\boldsymbol{A}(\tau)\cdot\boldsymbol{p} + \frac{1}{2}\boldsymbol{A}^2(\tau)\right] \times\exp\left[\mathrm{i}(S_{\boldsymbol{p}}(\tau) - E_\mathrm{i}\tau)\right]\widetilde{\Psi_\mathrm{i}}\left(\boldsymbol{p}_\perp, \boldsymbol{p}\cdot\hat{\boldsymbol{k}} - \alpha(E_p - E_\mathrm{i})\right), \tag{13}$$

in which the Volkov phase

$$S_{\boldsymbol{p}}(\tau) = \int^{\tau}\mathrm{d}t\left\{E_p + \left[\boldsymbol{A}(t)\cdot\boldsymbol{p} + \boldsymbol{A}^2(t)/2\right]/\left[1-\alpha(\boldsymbol{p}\cdot\hat{\boldsymbol{k}})\right]\right\}, \tag{14}$$

$$\widetilde{\Psi_\mathrm{i}}(\boldsymbol{p}) = \int\mathrm{d}\boldsymbol{r}\exp(-\mathrm{i}\boldsymbol{p}\cdot\boldsymbol{r})\Psi_\mathrm{i}(\boldsymbol{r}), \tag{15}$$

with $\phi_0(\boldsymbol{r})$ being the ground state wavefunction.

In Eq. (13), only the nondipole correction up to $O(\alpha)$ has been kept and higher-order relativistic corrections have been neglected. The expression form of Eq. (13) can be turned into other variants through an appropriate gauge transformation. For more details about these different expressions of the transition amplitude beyond the dipole approximation, we refer the readers to Refs. [77,79,179,180].

2.4. Numerical solution to time-dependent Schrödinger equation

Numerically solving the time-dependent Schrödinger equation (TDSE) based on the Hamiltonian (4) is a popular method to account the lowest-order nondipole corrections in light-matter interaction. In this case, the cylindrical symmetry is broken and thus one faces a truly three-dimensional problem. As usual, the wavefunction $\Psi(\boldsymbol{r},t)$ can be expanded in the spherical harmonics $\mathrm{Y}_{lm}(\theta,\phi)$ in the angular coordinates, which leads to a set of coupled differential equations for the radial wavefunctions,

$$\Psi(\boldsymbol{r},t) = \sum_{l=0}^{\infty}\sum_{m=-l}^{l}\frac{\Phi_{lm}(r,t)}{r}\mathrm{Y}_{lm}(\theta,\phi). \tag{16}$$

The resultant Schrödinger equation for the radial coefficients Φ_{lm} can be solved using various discretization methods.[181,182] In our previous work, we used the "finite difference method" to discretize the radial coordinate and the split-operator technique for the short-time propagator.[183] The initial state is obtained by an imaginary time propagation in the absence of the external field until the ground state energy and wave function are both fully converged.

After the end of the external fields, we get the final wavefunction $\Psi_\mathrm{f}(\boldsymbol{r})$ and project it onto the scattering state $\Psi_{\boldsymbol{p}}^{(-)}(\boldsymbol{r})$. Then the differential distribution of the ionized electron with a final momentum $\boldsymbol{p}$ is given by

$$\begin{aligned} P(\boldsymbol{p}) &= \left|\left\langle\Psi_{\boldsymbol{p}}^{-}|\Psi_\mathrm{f}\right\rangle\right|^2 \\ &= \left|\frac{1}{\sqrt{2\pi}p}\sum_{l,m}\int_0^{\infty}\mathrm{d}r(-\mathrm{i})^l\mathrm{e}^{\mathrm{i}(\sigma_l+\delta_l)}r \right. \\ &\quad \left. \times R_{pl}(r)\Phi_{lm}(r)\mathrm{Y}_{lm}(\hat{\boldsymbol{p}})\right|^2, \end{aligned} \tag{17}$$

in which $R_{pl}(r)$ are the radial wave functions of $\Psi_{\boldsymbol{p}}^{(-)}(\boldsymbol{r})$.

For the two-electron atom of helium, the Hamiltonian beyond the dipole approximation in multipole gauge is given by

$$\begin{aligned} H_\mathrm{VG} &= H_0 - \sum_{j=1,2}\mathrm{i}\boldsymbol{A}(t)\cdot\nabla_j - \mathrm{i}\alpha\left(\hat{\boldsymbol{k}}\cdot\boldsymbol{r}_j\right)\left[\boldsymbol{E}(t)\cdot\nabla_j\right] \\ &\quad + \alpha\left(\hat{\boldsymbol{k}}\cdot\boldsymbol{r}_j\right)\left[\boldsymbol{A}(t)\cdot\boldsymbol{E}(t)\right] + O(\alpha^2), \end{aligned} \tag{18}$$

where H_0 is the field-free Hamiltonian for the two electrons in helium and the interaction Hamiltonian is in the velocity gauge, with $\boldsymbol{L} = \boldsymbol{l}_1 + \boldsymbol{l}_2$ being the total angular momentum of electrons.

Similarly, the two-electron wavefunction can be expanded into a set of coupled spherical harmonics which is in

the time-dependent close-coupling (TDCC) scheme,[182]

$$\Psi(\boldsymbol{r}_1,\boldsymbol{r}_2,t)=\sum_{L,M,l_1,l_2}\frac{R^{L,M}_{l_1,l_2}(r_1,r_2,t)}{r_1r_2}\mathrm{Y}^{L,M}_{l_1,l_2}(\Omega_1,\Omega_2), \quad (19)$$

with the radial coordinates also discretized by finite-element discrete variable representation (FE-DVR) method. The wavefuction can be evolved using the Lanczos propagation algorithm.[184,185] The initial state is calculated by solving eigenvector of the Hamiltonian in Krylov subspace and the final scattering state is approximated by symmetrical product of single electron continuum with the incoming boundary condition. The differential distribution of the two ionized electrons can thus be computed.

For the two-center problem of a molecule, it is convenient to solve the corresponding TDSE in the spheroidal coordinates. The readers can get more details from Ref. [165] and references therein. Of course, in the perturbative regime, one can also develop a few-photon time-dependent perturbation theory in this coordinate system.

3. Nondipole phenomena in perturbative regime

3.1. Asymmetry in photoelectron angular distribution

According to Cooper's derivation,[43,44] the differential cross section of photoelectrons ejected from an isotropic system, or an anisotropic system but randomly orientated such as atoms or molecules in the gas phase can be written as

$$\frac{\mathrm{d}\sigma}{\mathrm{d}\Omega}=\frac{\sigma}{4\pi}\left[1+\beta\mathrm{P}_2(\cos\theta)+(\delta+\gamma\cos^2\theta)\sin\theta\cos\phi\right], \quad (20)$$

where P_2 is a Legendre polynomial, θ is the angle between the polarization of the light and the ejection direction of an electron, and ϕ is the angle between the photon propagation direction $\hat{\boldsymbol{k}}$ and the projection of $\boldsymbol{p}$ onto the plane perpendicular to laser polarization. σ is the total ionization cross section and β is the dipole anisotropy factor. The usual experimental scheme to measure those anisotropy parameters is to set $\theta=\arccos\sqrt{1/3}\approx 54.7^\circ$ (so $\mathrm{P}_2(\cos\theta)=0$) and to measure the differential cross sections σ_1 and σ_2 at $\phi=0^\circ$ and $\phi=90^\circ$ respectively, which satisfy

$$\frac{\sigma_1}{\sigma_2}=1+\sqrt{\frac{2}{27}}(3\delta+\gamma), \quad (21)$$

providing the indicated combination $\zeta=3\delta+\gamma$.

The first two terms on the right of Eq. (20) contribute to the usual dipole signal. In the perturbative regime, the nondipole angular-distribution parameters characterize the leading-order corrections to the dipole approximation. Specifically, γ represents the major correction term corresponding to the electric dipole–quadrupole interference and δ represents the magnetic–electric-dipole term. The nondipolar asymmetry in PADs is shown in Fig. 1 and the dependence of the nondipolar asymmetry parameter γ on energy and atomic subshell is confirmed in Refs. [30–32,42].

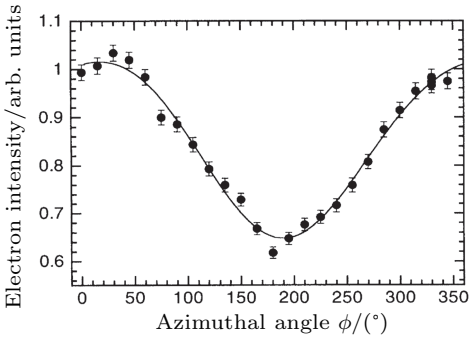


Fig. 1. Dependence on azimuthal angle ϕ of Ar 1s photoelectrons at the photon energy of 2000 eV. The polar angle is fixed at $\theta=54.7^\circ$. The solid line is a fitted curve used to determine the nondipolar asymmetry parameter γ. Source: Krässig *et al.*[31]

The significance of higher-order nondipole effects, *e.g.*, the pure-quadrupole and octupole–dipole interference terms, has also been demonstrated in PADs by a soft-x-ray pulse.[45] In this case, the vector potential of Eq. (3) should be expanded to include higher-order terms. Then the spin–magnetic coupling becomes spatially dependent and the spin–orbit coupling is comparable with the second-order nondipole terms. Therefore, both of them need to be included in theoretical models and the electronic spin may play an important role in the exhibition of higher-order nondipole effects.[151–155] At an extremely low energy, obvious nondipole effects have been observed in PADs due to a dipole-forbidden resonance enhancement,[48–58] in which situations the dipole transition amplitude is usually small around a dipole Cooper minimum.[59] Calculations and measurements[55,186,187] have verified the existence of the quadrupole Cooper minima according to the photoelectron asymmetry parameters.

In the ionization process, the nondipole path leads to a partial wave of different angular momenta, and it has been understood for many years that nondipole effects can be observed in the PAD for the single electron system.[44] For two-electron systems, there exist additional features: (i) there could be a nondipole resonance resulting in the magnification of nondipole effects; (ii) core relaxation exists and brings a nonzero parameter δ in PADs; (iii) the total angular momentum and energy are shared between two electrons with the consideration of the correlation, so for a nonsequential process the formula of PAD for the single-electron case becomes invalid, and one has to look at the double differential cross section (DDCS). In 2003, the observation of PAD in helium photoionization[51,52] confirmed the nondipole parameter can be enhanced by the quadrupole Fano resonance (which does not exist in single electron systems), and a good agreement between the *ab initio* calculations and experimental measurements was achieved. After several years, the DDCS (simi-

lar to PAD with a varying energy) of the single photon double ionization (SDPI) is theoretically investigated with the lowest-order perturbation theory and the convergent close-coupling theory (CCC),[188] revealing a nonzero parameter δ, which is usually zero for a single electron photoionization from 1s state.[44] Recently, the nondipole PAD parameters were experimentally observed in the two photon double ionization (TPDI) process in a sequential region using FELs at FERMI,[58] compared with theoretical calculations developed by Grum-Grzhimailo *et al.*[56,189] This study reveals a large nondipole parameter $\gamma_2^{(2)} = 0.47$ for the second electron at the Cooper minimum of Xenon, despite of existing discrepancy between theory and experiment.

In the XUV region, the single photon double ionization of helium atom has been well studied with dipole approximation, for reviews, see Refs. [190,191]. However, when the photon energy reaches hundreds of eV, the nondipole effects become pronounced. In 2004, Istomin *et al.* reported their calculations for nondipole effects in VUV region.[192] At an excess energy as low as 80 eV, a forward–backward asymmetry in the triply differential cross section (TDCS) was confirmed with a linearly polarized light. The case of an elliptically polarized light was discussed in the same year,[193] and they found that for the equal energy sharing, the circular dichroism exists, which is expected to be zero within the dipole approximation. Later, the details of their methods were published,[194] in which the electron's evolution is separately calculated with the ground state correlation and the final state correlation included. They showed TDCS at different geometries at an excess energy of 20, 100, and 450 eV, but their absolute TDCSs failed to get agreement with the the experimental results at excess energy of 450 eV. However, the ratio of the difference of the TDCSs in the forward and backward half-planes to the TDCS in the forward half-plane (Eq. (69) in Ref. [194]) is in a qualitative agreement. Considering the drawbacks of LOPT in handling the electron correlation, they investigated the TDCS at an excess energy of 450 eV with CCC method in 2006,[195] showing an improved agreement with the experiment measurements.

Besides these work by Istomin and coworkers, there were also several investigations on the nondipole effects in helium. Meharg *et al.* developed the time-dependent close-coupling method (for a review, see Ref. [196]) in the full-dimensionality and presented the applications for helium and hydrogen in intense IR laser fields. It should be noted that they dropped the term $-\mathrm{i}\boldsymbol{A}^{(1)}(\boldsymbol{r},t)\cdot\nabla/\mathrm{c}$ in the Hamiltonian, and the calculation for helium in this regime of laser parameters is very demanding even for computational facilities nowadays since it will involve too many partial waves. For nondipole effects in non-sequential double ionization of helium, Emmanouilidou and coworkers have taken the first step, using the classical trajectory Monte Carlo (CTMC) approch.[197] Later they reported the asymmetry of the transverse momentum of the tunneling electron introduced by the magnetic field, and explained the variation of the average momentum along the light propagation direction through analyzing the asymmetry.[198] In 2009, Ludlow and coworkers carried out the TDCC calculations beyond the dipole approximation at a photon energy of 800 eV.[199] Unfortunately, the nondipole contribution to the TDCS was considerably overestimated, possibly due to the drawback of their Hamiltonian, in which the light is not a transverse wave.

The early studies about nondipole effects in molecular PADs focused on the randomly oriented molecules. The first observation of a significance nondipole effect on molecule was made for N_2 in 2001.[60] They measured the ζ parameter for the photoelectron ionized from K-shell with a photon energy about hundreds of eV. A large nondipole signal (ζ close to one) was observed for a near-threshold ionization with photoelectron energy around 50 eV. A corresponding theoretical calculation[200,201] was performed based on the fixed-nuclear and the frozen-core Hartree–Fock (HF) approximation, and the main feature can be repeated from the computation. The resonance peak near the threshold is contributed by the σ^* resonance of the dipole transition moment with photoelectron energy around 10 eV,[202,203] which comes from the multiple-electron correlation, though their positions do not coincide with each other. In the next year, a coincidence experiment was carried out where the angular distribution for fixed-in-space N_2 (Ref. [61]) was measured at 660-eV photon energy for the K-shell photoelectron. A clear asymmetric structure can be directly seen from the angular distribution, as shown in Fig. 2. Due to the deviation between the theoretical calculation up to the first-order nondipole correction and the experimental result, they suggested that the higher order correlation should be taken into account. Measurements and calculations for nondipole parameters of photoelectrons from other shells of N_2 (Refs. [63,65]) and H_2 (Ref. [71]) were done later by the same group.

However, an independent experiment performed at the Photon Factory in Tsukuba, Japan[68] showed a negligible nondipole effect for the near-threshold ionization of K-shell electron from N_2. Their computation based on the relaxed-core HF with the random phase approximation (RPA) for the electron correlation confirmed their experimental observation. A similar conclusion for C K-shell of CO was also obtained.[67]

The third experiment was carried out at the Elettra synchrotron radiation source, Italy.[204] Together with their theory based on the density functional theory (DFT) with the single center expansion,[66] their results are consistent with

the Japanese group. Oscillation of nondipole parameters with photo energy from σ_g and σ_u states was observed theoretically, which can be understood with the classical Cohen–Fano model:[205] electrons emitted from the two nuclei interfere with each other, resulting in an oscillation factor of $e^{ip\cdot R}$, where $\boldsymbol{p}$ and $\boldsymbol{R}$ are the electron momentum and internuclear distance respectively. Since the energy of these two states are too close to be distinguished, there were no such indications in the experiment. Later they applied the multicentric basis set[206] to evaluate nondipole parameters for more complex molecules, include SF_6 (Ref. [207]) and C_{60} (Ref. [208]).

Aside from the debates on N_2, there were many theoretical works focused on nondipole effect of other molecules. Grum-Grzhimailo[62] reformulated the theory of angular distributions and angular correlations of photoelectrons and recoil ions in the molecular photoionization in terms of the density matrix and statistical tensor formalism, which incorporates a full multipole expansion of the radiation field. This theory was applied to compute the nondipole correlation for N 1s photoionization of NO (Refs. [70,209] and the circular dichroism in the molecular ion orientation distribution.[69] Seabra *et al.*[64] computed the nondipole correlation at photo energy of several keV for various molecules with the HF and the random phase approximation, including CH_4, NH_3, H_2O, and HF. Brumboiu *et al.*[210] calculated the nondipole ionization cross section for molecules with various of sizes by using the Gaussian-type orbitals for initial state and plane waves for final states. Baltenkov *et al.*[211] turned back to the single electron case, giving an analytic solution to the photoionization from a diatomic molecule with a zero-range potential, which provided some physical insights to the two-center nondipole effects.

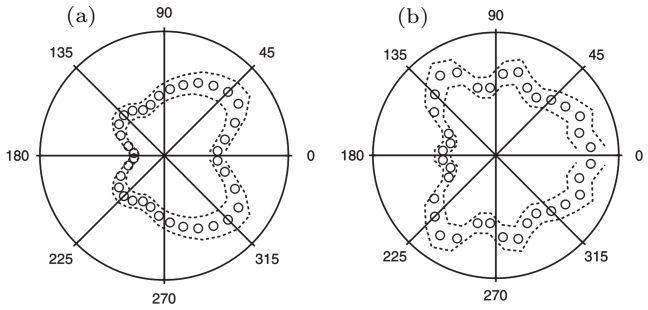


Fig. 2. Photoelectron angular distributions measured for parallel (a) and perpendicular (b) molecular orientations at photon energy of 660 eV. The dashed lines represent the statistical error. In panel (a) the molecular axis points out of the paper, while in panel (b) the molecular axis is aligned along the 90°–270° axis. Source: Guillemin *et al.*[61]

3.2. Photon momentum transfer in few-photon ionization

Photoionization of an atom by a photon with energy ω involves absorption of the photon's linear momentum $\boldsymbol{k}$, which is usually neglected in the atomic, molecular and optical physics due to its extreme smallness. The photon momentum transferred to the photoelectron can be extracted from the three-dimensional (3D) photoelectron momentum distribution $P(\boldsymbol{p})$, which have been calculated by one of the semiclassical or quantum mechanical numerical methods surveyed in Section 2. To be specific, the average photoelectron momentum along the laser propagation is given by

$$\overline{p}_k = \frac{\int (\boldsymbol{p}\cdot\hat{\boldsymbol{k}})P(\boldsymbol{p})\,\mathrm{d}^3\boldsymbol{p}}{\int P(\boldsymbol{p})\,\mathrm{d}^3\boldsymbol{p}}. \tag{22}$$

Under the dipole approximation, one obtains no net momentum transfer to the electron, thus $\overline{p}_k = 0$. However, even in the weakly relativistic regime, $\overline{p}_k$ becomes obviously non-zero and the interference between the dipole and quadrupole terms matters in calculating the fraction of the photon momentum transferred to the electron.

Within the perturbative regime, the momentum transfer in the photoelectric effect for the electron ionized from the ground state of the hydrogenlike atom is

$$\overline{p}_k = 1.6\alpha\overline{E}_p, \tag{23}$$

which can be deduced by the LOPT and verified by solving the TDSE.[76,77,79,80] The momentum given to the electron in the photoelectric effect is larger than the single photon momentum and has been demonstrated coming from the inhomogeneous electric field instead of the magnetic field since the magnetic number of the ground state of hydrogenlike atom is zero.[165] For one-photon ionization from different initial states, similar linear relationships with Eq. (23) can be obtained but with different slopes.[77,79,80] Please note that, the plane wave approximation for the final state can be only used in the derivation of the momentum transfer law for one-photon ionization from hydrogenlike 1s state. This approximation will introduce obvious discrepancies in calculations for any other initial states, in which cases one should adopt the scattering state as the final state.

Things would be much more complex for other systems, *e.g.*, molecules and two-electron systems. The average momentum of the ionized electron is not necessarily collinear with the photon momentum, since the interaction between the electron and the residual ions can be anisotropic. Lao *et al.*[212] provided an expression of photo momentum transfer for the diatomic molecule with zero-range potential. Liang *et al.*[165] carried out *ab initio* calculations on the nondipole correlation of H_2^+ within the fixed-nuclear approximation for various internuclear distances R. A relative large enhancement of photo momentum transfer than H atom was found for near the threshold region as shown in Fig. 3. Diagonal patterns represent previously mentioned interferences between the two nuclei, and the divergence to the white parallel lines $p_eR = \text{const}$, indicating the influence of long-range Coulomb potential.

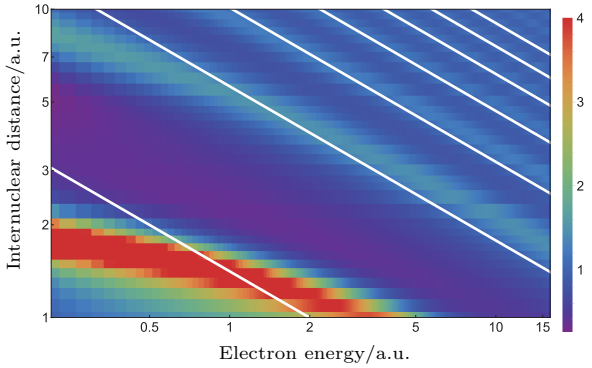


Fig. 3. The ratio between the average momentum transfer from H_2^+ to that from H atom in the (E,R) plane, plotted in a double logarithmic scale. White straight lines with a slope equal to $-1/2$ are plotted for reference. Source: Liang *et al.*[165]

About 44 years ago, Amusia *et al.* took nondipole effects into account in the single photon double ionization, predicting the so called quasi-free mechanism (QFM),[213] by which the electrons can break the well-known selection rules within the dipole approximation that the equal energy sharing back-to-back emission is forbidden.[190] The details of QFM can be found in Ref. [214]. In 2012, Galstyan *et al.* calculated the nondipole effects by the perturbatiion theory with the final state described by the three-body double-continuum Coulomb function (3C) and the uncorrelated 2C function.[215] Their results showed the breakdown of the selection rules mentioned above, and this effect is strongest in helium than other helium-like atoms. When electrons with an equal energy sharing emit back-to-back, the ion momentum equals to the photon momentum absorbed in the photon ionization process, which is about 0.2 a.u. for a photon energy at 800 eV, and the typical ion momentum from the dipole path is about 6 a.u. in this situation. As a result, the yield of ions which have a momentum close to zero is a sign of the nondipole effects. Schöffler *et al.*[216] observed such a phenomenon in 2013 at photon energies of 440 eV and 800 eV, but their theoretical calculations by CCC and TDCC method overestimated the nondipole effects (*i.e.*, the yield of ion momentum close to zero is as strong as the dipole yield). Five years later, they managed to realize kinematically complete measurement of SPDI, reported the differential cross section for the coplanar geometry and equal sharing, in which the back-to-back emission can be clearly seen and separated from the dipole yield, and the experiment is in great agreement with the CCC theory.[217]

In Ref. [218], the photon momentum transfer in the single-photon double ionization of helium is investigated experimentally and theoretically. Their main conclusions are shown in Fig. 4, where the lines in the figure are linear fitting. The observables are the average momentum along the light propagation direction, with their carriers defined as: $\langle k_z^{\rm total}\rangle$, for undistinguished single electrons; $\langle k_{\rm fast}\rangle$, for electrons with more kinetic energy than the other one; $\langle k_{\rm slow}\rangle$, for electrons with less or equal kinetic energy than the other one; $\langle Q_z\rangle$, for the helium ion. The experimental measurements agree well with the numerical results, giving rough rules that $\langle k_{\rm fast}\rangle \approx 1.7\alpha E_{\rm ex}$, $\langle Q_z\rangle \approx -0.7\alpha E_{\rm ex} + \alpha I_p$, in which $E_{\rm ex} = \omega - I_p$ and the momentum for slow electrons is negligible than the fast electrons and ions. The slope of $\langle k_{\rm fast}\rangle$ is close to 1.6α (the slope for hydrogen 1s state). From a further analysis of the average electron momentum at a certain energy sharing (*cf.*, Fig. 2 of Ref. [218]), we find that each of the two electrons, whether it is the shake-off, the knock-out, or the primary photoelectron, receives its share of 8/5 of its energy. The only exception are electrons freed by the quasi-free mechanism.

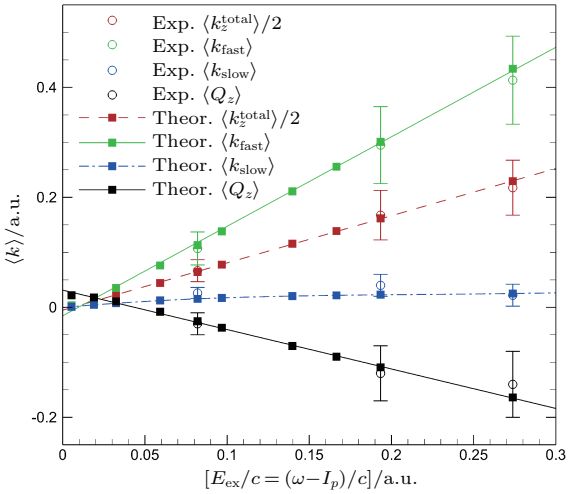


Fig. 4. The average momenta for the electrons and the ion along the direction of the light propagation as functions of the excess energy divided by light speed $E_{\rm ex}/c = (\omega - I_p)/c$. Source: Chen *et al.*[218]

In the atomic two-photon ionization, the total cross sections and angular distributions of electrons beyond the dipole approximation have been widely discussed for a long time.[219–227] Numerical fitting shows that a good linear relationship like Eq. (23), namely $\overline{p}_k = 1.7\alpha\overline{E}_p$, persists for circularly polarized lasers.[78–80] The slight difference in slopes can be understood by the second transition from the intermediate states to the continuum state in the two-photon ionization because radiative pressure effects in the single-photon ionization for other initial states differ from that for the hydrogen ground state.[76,79,80] However, Wang *et al.*[80,81] identified a series of minimums in the photon-momentum transfer of two-photon ionization for a linear-polarized pulse, as shown in Fig. 5. The minima locate between two adjacent resonant peaks of two-photon ionization. The depth of these minima will decrease with the increase of the laser field ellipticity and they will disappear in circularly polarized external fields. The underlying mechanisms have been revealed through a time-dependent perturbation theory beyond the dipole approximation and the TDSE calculations. The ratio of the probability of each dipole transition pathways to the total ionization probability oscillates with the increase of the photon energy and those dipole

transition pathways interfere with the nondipole ones, which jointly lead to the minima in the linear momentum transfer for the case of the linear polarization.

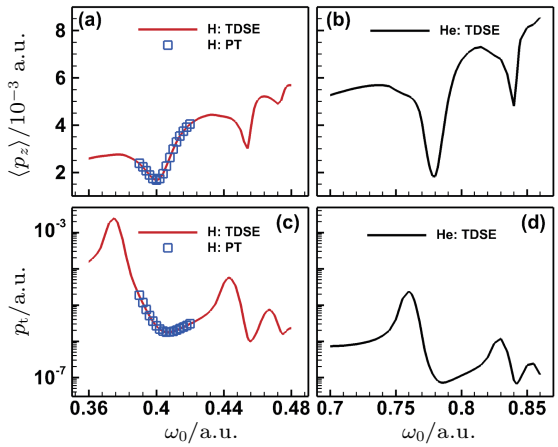


Fig. 5. The laser pulse polarizes along the x axis and propagates along the z axis thus $\overline{p}_k = \langle p_z \rangle$ for (a) the hydrogen and (b) the helium atomic system. The two-photon ionization probability is shown as a function of the central frequency ω_0 for panel (c) the hydrogen and (d) the helium atomic system described by a model potential.[228] The square symbols in panels (a) and (c) are results from the perturbation theory (PT). Source: Wang *et al.*[81]

4. Nondipole phenomena in strong field regime

4.1. Linear momentum transfer in tunneling ionization

By increasing the laser intensity of the IR or Mid-IR light, Smeenk *et al.*[82] and Ludwig *et al.*[88] have successively reported experimental observations of a photoelectron momentum shift along the direction of laser propagation in the tunneling ionization process. Theoretical works have confirmed this asymmetrical electron momentum distribution and a nonzero momentum shift along the laser's propagation direction by quantum-mechanical calculations,[83,91] semiclassical models with the Lorentz force included,[84,88,92] solution to the time-dependent Dirac equation,[90] and strong field approximation models beyond the dipole approximation.[77,79,128,180] The pioneering work by Chelkowski *et al.*[77] has predicted different photon-momentum partitioning rules for one-photon ionization and multiphoton processes, the former of which has been discussed above and the latter of which has been supported by a recent experiment.[229] Within the long-wavelength limit of a linearly polarized light, the Coulomb interaction and the rescattering events may result in a momentum shift opposite to the direction of laser propagation,[79,88,92] particularly for the low-energy electrons. Besides, the under-barrier motion caused by the laser–magnetic-field-induced Lorentz force has been reported to be relevant to the electron momentum shift in the laser propagation direction.[86,87,89,95]

In the tunneling regime, figure 6(a) from the experimental work[82] shows that the photon momentum transferred to the ionized electron grows linearly as a function of the laser intensity. A classical description is used to interpret the experimental observation, which shows that the average of photoelectron momentum component along the laser propagation equals the electron's drift kinetic energy divided by the light speed. It claims that no net momentum comes from the ponderomotive energy and the momentum αI_p corresponding to photons necessary to overcome the ionization energy is totally transferred to the ion not to the electron. Similar results have been reported in several other theoretical works.[83–85]

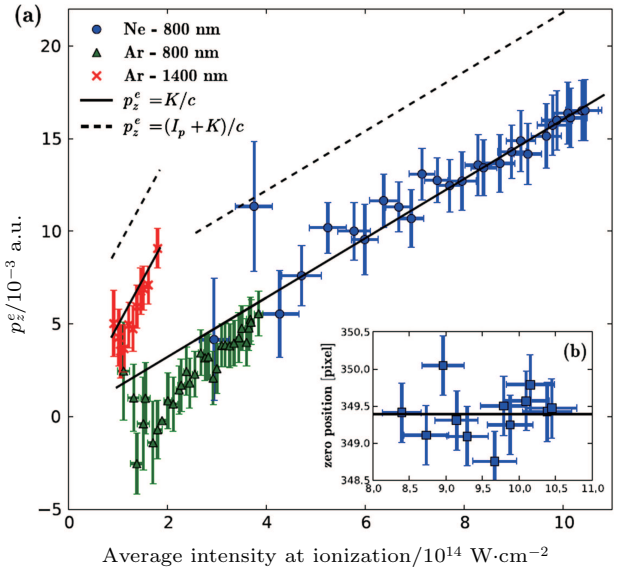


Fig. 6. (a) The center of the electron momentum distribution along the laser propagation direction as a function of the average intensity of the light. The theory lines are given by $p_z^e = K/c$. (b) The zero position of the momentum distribution along the z axis as a function of laser intensity. Source: Smeenk *et al.*[82]

However, a constant net momentum shift equal to $0.3\alpha I_p$ has been proposed in theoretical works mainly based on the SFA,[77,79,86,87] which makes the partition rule in the tunneling regime change into

$$\overline{p}_k = \alpha \overline{E}_p + 0.3\alpha I_p. \tag{24}$$

According to the momentum conservation law, only the momentum around $0.7\alpha I_p$ is transferred to the residual ion. This tiny shift, absent in the experimental results of Ref. [82] because of the experimental uncertainties while measured in a recent experiment,[229] has been claimed to stem from the under-barrier dynamics of the electron.[86] Equation (24) is totally different from the photon momentum transfer rules showed in Eq. (23) for the single-photon ionization. To investigate the expected linear momentum shift between the short- and long-wavelength limit, He *et al.*[79] defined a formulation as

$$\overline{p}_k = \frac{\alpha' \overline{E}_p + \beta I_p + \gamma U_p}{c}, \tag{25}$$

where α', β, and γ are fitting parameters depending on the necessary absorbed photon number N. The changes in the value of

(α', β, γ) from the hydrogen ground state by a laser at the intensity of 10^{14} W/cm^2 in Fig. 7 indicate the nondipole effects in different regimes.

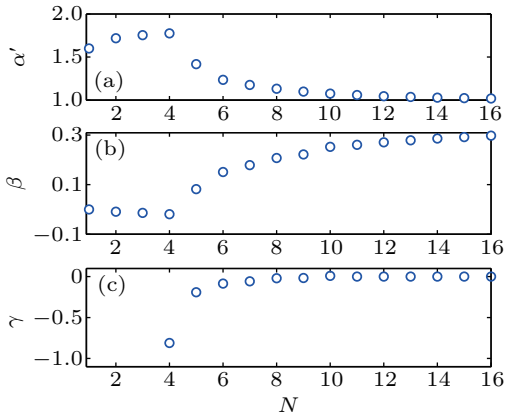


Fig. 7. The fitted (a) α', (b) β, and (c) γ as a function of the necessary absorbed photon number N. Source: He *et al.*[79]

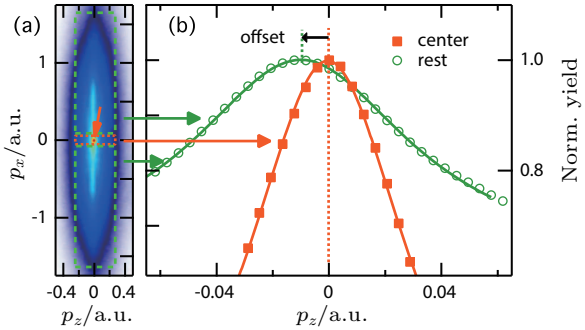


Fig. 8. (a) Typical projected photoelectron momentum distribution of xenon recorded at an intensity of 6×10^{13} W/cm^2 with linear polarization along x axis and at a center wavelength of 3.4 μm. The orange arrow is used as reference for $p_z = 0$ a.u. and the dashed boxes indicate the areas taken for the momentum-offset analysis. (b) Projections of the PMD onto the beam propagation direction (z axis) together with Lorentzian fits. The orange curve (squares) is used to set the $p_z = 0$ a.u. reference and the offset of the maximum of $f(p_z)$ is extracted from the fit on the green markers (circles). Source: Ludwig *et al.*[88]

Besides the momentum transfer law in the long-wavelength limit, Ludwig *et al.*[88] experimentally observed an increasing shift of the peak of $f(p_z)$ opposite to the beam propagation direction (z axis) with increasing laser intensities of the linearly-polarized pulse, as shown in Fig. 8. Similar results have also been reported in a recent experimental work,[94] in which the momentum shift varies from being negative (which means opposite to the beam propagation direction) at small ellipticities to being positive at higher ellipticities of the external light, see Fig. 9. This counterintuitive laser intensity- and ellipticity-dependent shift of the photoelectron momentum cusp is attributed to the complex interplay of the external laser pulse and the Coulomb potential by theoretical works based on the nondipole SFA theory,[79,230] classical[92,93,231] and quantum[232] trajectory Monte Carlo calculations and TDSE simulations.[91] In more detail, an analytical formula in Ref. [93] indicates that the average drift momentum due to the laser magnetic field until the single recollision leads to the negative shift of the cusp, which however will be decreased by the multiple rescattering events. It has been theoretically predicated in Refs. [91,233] that such combined effect of Coulomb focusing and the laser magnetic-field-induced drift in the beam propagation direction can cause a discernible asymmetry in the holographic interference pattern as well. Recently, Willenberg *et al.*[232] have theoretically and experimentally confirmed similar asymmetries and derived analytical laws for the nondipole momentum shift of the holography interference pattern.

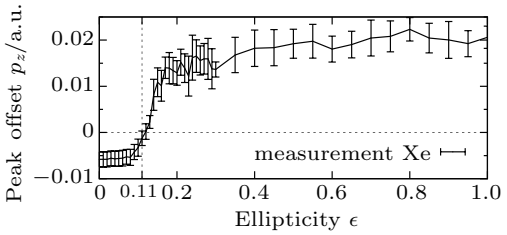


Fig. 9. Peak offset of the complete projection of the measured PMDs onto the beam propagation direction (z axis) as a function of ellipticity at constant intensity. A transition from negative to positive values of the peak offset is observed with a zero crossing at $\varepsilon \approx 0.12$. Source: Maurer *et al.*[94]

4.2. Nondipole effects in atomic dynamic interference

Nondipole effects for the one-photon ionization in the perturbative regime are discussed in Subsection 3.2. With a sharp increase in the laser intensity, highly non-perturbative electronic dynamics will appear, such as the atomic stabilization and the dynamic interference. In the stabilization region, the single-photon ionization rate no longer increases with the laser intensity as predicted by the LOPT, but is strongly suppressed, resulting in the survival rather than ionization of atomic bound states. The stabilization effect is expected to occur in the atomic single-photon ionization at super-high laser intensities, *i.e.*, intensities of more than 10^{16} W/cm^2 for atomic hydrogen.[102,121,122] In the external field at a moderately high frequency ($\sim$ 50 eV) and a super-high intensity (above 10^{18} W/cm^2), the atomic stabilization is expected to occur and thus makes the dynamic interference possible for the ground state of hydrogen, which refers to the interference between two electronic wave packets respectively ejected in the rising and the falling edge of a laser pulse.[119]

According to the Einstein's photoelectric law, a single peak at the energy of $\omega - I_p$ is expected in the photoelectron energy spectrum for one-photon ionization in the perturbative process. However, the single peak can gradually evolve into a multi-peak structure due to the dynamic interference when the laser intensity is increased to reach the nonperturbative regime, see the photoelectron energy distribution $D(E)$ at various laser intensities in Figs. 10(a)–10(d).

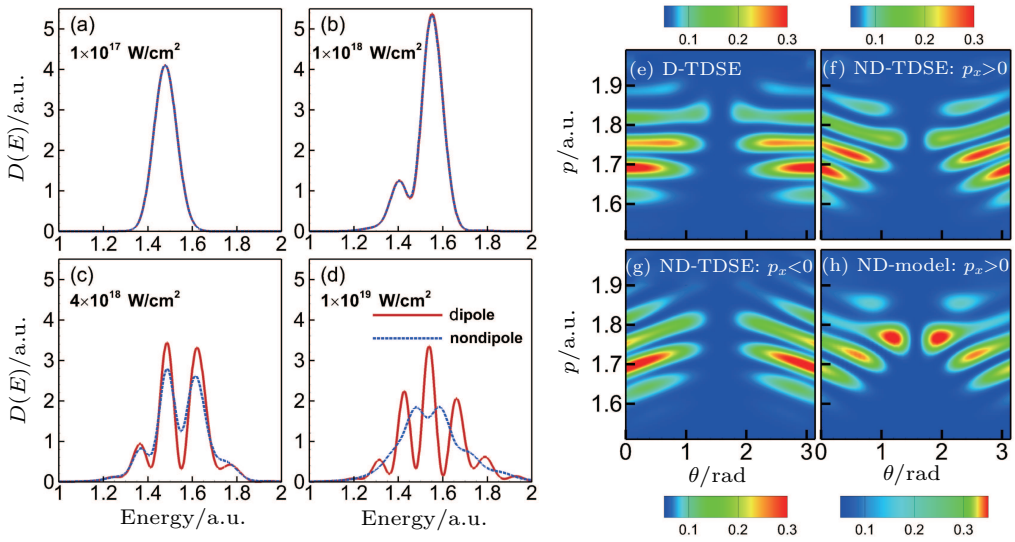


Fig. 10. The photoelectron energy distribution (PED) for the 1s hydrogen state exposed to linearly polarized Gaussian-shaped pulses with a carrier frequency of $\omega = 53.6$ eV and FWHM of 7 cycles at four different laser intensities: (a) $I_0 = 1.0 \times 10^{17}$ W/cm^2, (b) $I_0 = 1.0 \times 10^{18}$ W/cm^2, (c) $I_0 = 4.0 \times 10^{18}$ W/cm^2, and (d) $I_0 = 1.0 \times 10^{19}$ W/cm^2. Red solid line: the dipole result; blue dotted line: the nondipole result. The PAD in the p_x–p_z plane ($p_y = 0$) at $I_0 = 1.0 \times 10^{19}$ W/cm^2 are shown for: (e) the dipole TDSE calculation, (f) the nondipole TDSE calculation for $p_x > 0$, (g) the nondipole TDSE calculation for $p_x < 0$, and (h) semi-analytical model results for $p_x > 0$. Source: Wang *et al.*[120]

In Fig. 10, the results from the dipole approximation are consistent with the previous studies,[119] *i.e.*, the dynamic interference does appear for pulse intensity above 10^{18} W/cm^2 even for the ground state of hydrogen, due to the atomic stabilization. However, for the present photon energy (~ 50 eV), the limit of the dipole approximation is approached at the laser intensity of 10^{19} W/cm^2 (see, *e.g.*, Fig. 4 in Ref. [7]) and the nondipole effects may be non-negligible. Drastic differences in the photoelectron energy distribution (PED) can be observed between the dipole and the nondipole results at higher intensities, see Figs. 10(c) and 10(d). The inclusion of the nondipole corrections can significantly suppress the peak splitting in the energy spectrum.

Detailed angularly distinguished momentum spectra of the photoelectron within/beyond the dipole application are presented, for example the momentum distributions in the polar coordinates of the polarization–propagation (p_x–p_z) plane in Figs. 10(e)–10(h). As shown in Fig. 10(e), the dipole results are identical for the electrons with $p_x > 0$ and $p_x < 0$. However with the nondipole corrections included, the angular distributions are drastically different for electrons with $p_x > 0$ and those with $p_x < 0$, as is respectively shown in Figs. 10(f) and 10(g): the momentum is shifted toward a smaller or a larger value. Such shifts in the momentum spectra destroy the symmetry of the interference structures and therefore significantly suppress the peak splitting in the angularly integrated energy spectrum in Figs. 10(c) and 10(d).

By including the nondipole corrections for the Volkov phase[79,106] into the semi-analytical model previously developed for the dynamic interference,[119] the momentum shift observed in the TDSE calculations is nicely reproduced, as is shown in Fig. 10(h) for $p_x > 0$. From the satisfactory agreement between Figs. 10(f) and 10(h), it is reasonable to attribute the origin of the momentum shift to the nondipole phase differences between electrons emitted in the rising and falling edge of the laser pulse, which will interfere with each other. Besides, an analytic expression for the momentum shift of the peak positions in the momentum spectra can be obtained,

$$\Delta p_{\text{peak}} \propto -\omega^{-2} I_0 \Delta p_0 p_x, \tag{26}$$

where I_0 is the laser peak intensity, Δp_0 is the interference fringe spacing, and p_x is the momentum component along the laser propagation direction. It can be seen in Eq. (26) that the nondipole peak shift is zero if $p_x = 0$ ($\theta = 0, \pi$). For $p_x \neq 0$, the nondipole effects will become significant and the momentum shift will depend on the sign of p_x. According to Eq. (26), Δp_{peak} is negative for electrons with $p_x > 0$ and positive for $p_x < 0$. This can explain the different trends of shifts in the momentum space for electrons with positive and negative p_x in Figs. 10(f) and 10(g).

4.3. Nondipole effects in high-order harmonic generation

In Subsection 4.1, we mentioned that the rescattering events could induce a negative nondipole shift of the photoelectron momentum cusp in the long-wavelength limit. Like the rescattering, the recombination process is also a hot topic in strong field phenomena, which comes from the three-step (*i.e.*, ionization, acceleration, and recombination) model[234–236] and can be used to understand the HHG process. With the laser wavelength and intensity increased to the weakly relativistic regime, the magnetic-field-induced drift of the photoelectron in the laser propagation direction becomes non-negligible[127,142,237–241] and may reduce the chance of the ionized electron revisiting the residual ion.[125–128] Thus

the recombination process will be influenced by the drift and nondipole effects will modify the HHG spectrum.

On one hand, for photons emitted along the laser polarization direction, calculations for He^+ ions by a semiclassical theory[138] indicate that the nondipole corrections can lead to a decrease of the high harmonic yield and a shift of the HHG spectra. Similar results have been obtained by a fully relativistic treatment[139,141,142] and theoretical works based on SFA.[140,142,143,145] In 2016, Zhu *et al.*[144] proposed different rules for the decrease of harmonic yield due to the nondipole effects in the high-intensity region and in the long-wavelength region respectively.

On the other hand, emitted photons have been found along the laser propagation direction, which is forbidden within the dipole approximation. Potvliege *et al.*[149] claimed that photon emission by He^+ ions along the propagation direction of a few-cycle laser pulse with wavelength of 800 nm and peak intensity of 5.6×10^{15} W/cm^2 was few orders of magnitude weaker than that along the laser polarization direction. Similar conclusions have been reported for hydrogen-like ions[140] and multiply charged ions.[150]

Besides, the magnetic-field component of the laser will break the symmetry of the system and even harmonics will appear in the spectra.[148] Vázquez *et al.*[146] have seen intense even harmonics emitted from a 3D hydrogen atom interacting with a high-frequency super-intense linearly polarized laser field. In 2006, Bandrauk *et al.*[147] presented the TDSE calculations of the nondipole effects in HHG for a Born–Oppenheimer 3D molecule H_2^+ exposed to a linearly polarized ultrashort intense XUV pulse. Even harmonics, which should not be emitted due to parity and symmetry considerations in the dipole approximation, were found generated by the magnetic component of the laser pulse in both parallel (laser-polarization) and perpendicular (laser-propagation) directions to the molecular axis.

5. Conclusions

The dipole approximation has been commonly used in the theoretical treatment of the laser pulse interacting with atoms and molecules. When the laser wavelength is comparable with the atomic size or when the photoelectrons can be accelerated to a considerable velocity at high laser intensities, this approximation fails and physical phenomena related to the nondipole effects become obvious. The inclusion of the nondipole corrections will break the symmetry of the system's Hamiltonian, which can be seen from theoretical models introduced above like numerically solving the time-dependent Schrödinger equation, the perturbation theory, the classical trajectory Monte Carlo method, and the strong field approximation. In this review, we have discussed the exhibition of the nondipole effects in both the perturbative and the non-perturbative regime, especially including topics such as the asymmetry photoelectron angular distributions, the photon momentum transfer, the dynamic interference, and high-order harmonic generation. Experimental and theoretical works in few-electron and molecular systems have been discussed.

References

[1] Göppert-Mayer M 1931 *Ann. Phys.* **9** 273
[2] Bandrauk A D, Fillion-Gourdeau F and Lorin E 2013 *J. Phys. B* **46** 153001
[3] Emma P, Akre R, Arthur J, *et al.* 2010 *Nat. Photon.* **4** 641
[4] McNeil B W J and Thompson N R 2010 *Nat. Photon.* **4** 814
[5] Ishikawa T, Aoyagi H, Asaka T, *et al.* 2012 *Nat. Photon.* **6** 540
[6] Young L, Ueda K, Gühr M, *et al.* 2018 *J. Phys. B* **51** 032003
[7] Reiss H R 2014 *J. Phys. B* **47** 204006
[8] Biegert J, Bates P K and Chalus O 2012 *IEEE J. Sel. Top. Quantum Electron.* **18** 531
[9] Wolter B, Pullen M G, Baudisch M, Sclafani M, Hemmer M, Senftleben A, Schröter C D, Ullrich J, Moshammer R and Biegert J 2015 *Phys. Rev. X* **5** 021034
[10] Elu U, Baudisch M, Pires H, Tani F, Frosz M H, Köttig F, Ermolov A, Russell P S J and Biegert J 2017 *Optica* **4** 1024
[11] Fu Y, Xue B, Midorikawa K and Takahashi E J 2018 *Appl. Phy. Lett.* **112** 241105
[12] Nie Z, Pai C H, Hua J, Zhang C, Wu Y, Wan Y, Li F, Zhang J, Cheng Z, Su Q, Liu S, Ma Y, Ning X, He Y, Lu W, Chu H H, Wang J, Mori W B and Joshi C 2018 *Nat. Photon.* **12** 489
[13] Kowligy A S, Timmers H, Lind A J, Elu U, Cruz F C, Schunemann P G, Biegert J and Diddams S A 2019 *Sci. Adv.* **5** eaaw8794
[14] Wilson D J, Summers A M, Zigo S, Davis B, Robatjazi S J, Powell J A, Rolles D, Rudenko A and Trallero-Herrero C A 2019 *Sci. Rep.* **9** 6002
[15] Tate J, Auguste T, Muller H G, Salières P, Agostini P and DiMauro L F 2007 *Phys. Rev. Lett.* **98** 013901
[16] Agostini P and DiMauro L F 2008 *Contemp. Phys.* **49** 179
[17] Colosimo P, Doumy G, Blaga C I, Wheeler J, Hauri C, Catoire F, Tate J, Chirla R, March A M, Paulus G G, Muller H G, Agostini P and DiMauro L F 2008 *Nat. Phys.* **4** 386
[18] Blaga C I, Catoire F, Colosimo P, Paulus G G, Muller H G, Agostini P and DiMauro L F 2009 *Nat. Phys.* **5** 335
[19] Wolter B, Pullen M G, Le A T, Baudisch M, Doblhoff-Dier K, Senftleben A, Hemmer M, Schröter C D, Ullrich J, Pfeifer T, Moshammer R, Gräfe S, Vendrell O, Lin C D and Biegert J 2016 *Science* **354** 308
[20] Reiss H R 2008 *Phys. Rev. Lett.* **101** 043002
[21] Di Piazza A, Müller C, Hatsagortsyan K Z and Keitel C H 2012 *Rev. Mod. Phys.* **84** 1177
[22] Sommerfeld A and Schur G 1930 *Ann. Phys.* (Leipzig) **4** 409
[23] Scofield J H 1989 *Phys. Rev. A* **40** 3054
[24] Trzhaskovskaya M B, Nikulin V K, Nefedov V I and Yarzhemsky V G 2001 *J. Phys. B* **34** 3221
[25] Krässig B, Bilheux J C, Dunford R W, Gemmell D S, Hasegawa S, Kanter E P, Southworth S H, Young L, LaJohn L A and Pratt R H 2003 *Phys. Rev. A* **67** 022707
[26] Isomura N, Kitazumi K, Kataoka K, Takahashi N, Kimoto Y and Dohmae K 2014 *J. Electron Spectros. Relat. Phenomena* **195** 62
[27] Simon M, Piancastelli M N and Lindle D W 2016 *Hard X-ray Photoelectron Spectroscopy (HAXPES)* (Springer, Cham: Joseph W) pp. 65–110
[28] Krause M O 1969 *Phys. Rev.* **177** 151
[29] Wuilleumier F and Krause M O 1974 *Phys. Rev. A* **10** 242
[30] Scofield J H 1990 *Phys. Scr.* **41** 59
[31] Krässig B, Jung M, Gemmell D S, Kanter E P, LeBrun T, Southworth S H and Young L 1995 *Phys. Rev. Lett.* **75** 4736
[32] Jung M, Krässig B, Gemmell D S, Kanter E P, LeBrun T, Southworth S H and Young L 1996 *Phys. Rev. A* **54** 2127
[33] Hemmers O, Fisher G, Glans P, Hansen D L, Wang H, Whitfield S B, Wehlitz R, Levin J C, Sellin I A, Perera R C C, Dias E W B, Chakraborty H S, Deshmukh P C, Manson S T and Lindle D W 1997 *J. Phys. B* **30** L727
[34] Lindle D W and Hemmers O 1999 *J. Electron Spectros. Relat. Phenomena* **100** 297

[35] Lee J J, Fisher C J, Woodruff D P, Roper M G, Jones R G and Cowie B C C 2001 *Surf. Sci.* **494** 166

[36] Hemmers O, Guillemin R, Kanter E P, Krässig B, Lindle D W, Southworth S H, Wehlitz R, Baker J, Hudson A, Lotrakul M, Rolles D, Stolte W C, Tran I C, Wolska A, Yu S W, Amusia M Y, Cheng K T, Chernysheva L V, Johnson W R and Manson S T 2003 *Phys. Rev. Lett.* **91** 053002

[37] Hemmers O, Guillemin R, Rolles D, Wolska A, Lindle D W, Cheng K T, Johnson W R, Zhou H L and Manson S T 2004 *Phys. Rev. Lett.* **93** 113001

[38] Guillemin R, Hemmers O, Lindle D W and Manson S T 2006 *Radiat. Phys. Chem.* **75** 2258

[39] Cooper J W and Manson S T 1969 *Phys. Rev.* **177** 157

[40] Tseng H K, Pratt R H, Yu S and Ron A 1978 *Phys. Rev. A* **17** 1061

[41] Bechler A and Pratt R H 1989 *Phys. Rev. A* **39** 1774

[42] Bechler A and Pratt R H 1990 *Phys. Rev. A* **42** 6400

[43] Cooper J W 1990 *Phys. Rev. A* **42** 6942

[44] Cooper J W 1993 *Phys. Rev. A* **47** 1841

[45] Derevianko A, Hemmers O, Oblad S, Glans P, Wang H, Whitfield S B, Wehlitz R, Sellin I A, Johnson W R and Lindle D W 2000 *Phys. Rev. Lett.* **84** 2116

[46] Trzhaskovskaya M B, Nefedov V I and Yarzhemsky V G 2002 *T. Data Nucl. Data Tables* **82** 257

[47] Nefedov V I, Yarzhemsky V G, Nefedova I S and Trzhaskovskaya M B 2000 *J. Electron Spectros. Relat. Phenomena* **113** 91

[48] Leuchs G, Smith S J, Dixit S N and Lambropoulos P 1986 *Phys. Rev. Lett.* **56** 708

[49] Martin N L S, Thompson D B, Bauman R P, Caldwell C D, Krause M O, Frigo S P and Wilson M 1998 *Phys. Rev. Lett.* **81** 1199

[50] Grum-Grzhimailo A N 2001 *J. Phys. B* **34** L359

[51] Krässig B, Kanter E P, Southworth S H, Guillemin R, Hemmers O, Lindle D W, Wehlitz R and Martin N L S 2002 *Phys. Rev. Lett.* **88** 203002

[52] Kanter E P, Krässig B, Southworth S H, Guillemin R, Hemmers O, Lindle D W, Wehlitz R, Amusia M Y, Chernysheva L V and Martin N L S 2003 *Phys. Rev. A* **68** 012714

[53] Lépine F, Zamith S, de Snaijer A, Bordas C and Vrakking M J J 2004 *Phys. Rev. Lett.* **93** 233003

[54] Dolmatov V K, Bailey D and Manson S T 2005 *Phys. Rev. A* **72** 022718

[55] Pradhan G B, Jose J, Deshmukh P C, LaJohn L A, Pratt R H and Manson S T 2011 *J. Phys. B* **44** 201001

[56] Gryzlova E V, Grum-Grzhimailo A N, Strakhova S I and Meyer M 2013 *J. Phys. B* **46** 164014

[57] Gryzlova E V, Grum-Grzhimailo A N, Kuzmina E I and Strakhova S I 2014 *J. Phys. B* **47** 195601

[58] Ilchen M, Hartmann G, Gryzlova E V, Achner A, Allaria E, Beckmann A, Braune M, Buck J, Callegari C, Coffee R N, Cucini R, Danailov M, De Fanis A, Demidovich A, Ferrari E, Finetti P, Glaser L, Knie A, Lindahl A O, Plekan O, Mahne N, Mazza T, Raimondi L, Roussel E, Scholz F, Seltmann J, Shevchuk I, Svetina C, Walter P, Zangrando M, Viefhaus J, Grum-Grzhimailo A N and Meyer M 2018 *Nat. Commun.* **9** 4659

[59] Cooper J W 1962 *Phys. Rev.* **128** 681

[60] Hemmers O, Wang H, Focke P, Sellin I A, Lindle D W, Arce J C, Sheehy J A and Langhoff P W 2001 *Phys. Rev. Lett.* **87** 273003

[61] Guillemin R, Hemmers O, Lindle D W, Shigemasa E, Le Guen K, Ceolin D, Miron C, Leclercq N, Morin P, Simon M and Langhoff P W 2002 *Phys. Rev. Lett.* **89** 033002

[62] Grum-Grzhimailo A N 2003 *J. Phys. B* **36** 2385

[63] Hemmers O, Guillemin R, Rolles D, Wolska A, Lindle DW, Kanter EP, Krässig B, Southworth SH, Wehlitz R, Langhoff PW, McKoy V and Zimmermann B 2005 *J. Electron Spectros. Relat. Phenomena* **144–147** 155

[64] Seabra G M, Kaplan I G and Ortiz J V 2005 *J. Chem. Phys.* **123** 114105

[65] Hemmers O, Guillemin R, Rolles D, Wolska A, Lindle D W, Kanter E P, Krässig B, Southworth S H, Wehlitz R, Zimmermann B, McKoy V and Langhoff P W 2006 *Phys. Rev. Lett.* **97** 103006

[66] Toffoli D and Decleva P 2006 *J. Phys. B* **39** 2681

[67] Hosaka K, Adachi J, Golovin A V, Takahashi M, Teramoto T, Watanabe N, Jahnke T, Weber Th, Schöffler M, Schmidt L, Osipov T, Jagutzki O, Landers A L, Prior M H, Schmidt-Böcking H, Dörner R, Yagishita A, Semenov S K and Cherepkov N A 2006 *Phys. Rev. A* **73** 022716

[68] Hosaka K, Adachi J, Golovin A V, Takahashi M, Teramoto T, Watanabe N, Yagishita A, Semenov S K and Cherepkov N A 2006 *J. Phys. B* **39** L25

[69] Grum-Grzhimailo A N, Lucchese R R, Prümper G and Ueda K 2007 *J. Electron Spectros. Relat. Phenomena* **155** 104

[70] Grum-Grzhimailo A N, Lucchese R R, Liu X J, Prümper G, Morishita Y, Saito N and Ueda K 2007 *J. Electron Spectros. Relat. Phenomena* **155** 100

[71] Zimmermann B, McKoy V, Southworth S H, Kanter E P, Krässig B and Wehlitz R 2015 *Phys. Rev. A* **91** 053410

[72] Kircher M, Rist J, Trinter F, Grundmann S, Waitz M, Melzer N, Vela-Perez I, Mletzko T, Pier A, Strenger N, Siebert J, Janssen R, Schmidt L Ph H, Artemyev A N, Schöffler M S, Jahnke T, Dörner R and Demekhin Ph V 2019 *Phys. Rev. Lett.* accepted

[73] Demekhin Ph V 2014 *J. Phys. B* **47** 025602

[74] Brumboiu I E, Eriksson O and Norman P 2019 *J. Chem. Phys.* **150** 044306

[75] List N H, Kauczor J, Saue T, Jensen H J A and Norman P 2015 *J. Chem. Phys.* **142** 244111

[76] Seaton M J 1996 *J. Phys. B* **29** 2373

[77] Chelkowski S, Bandrauk A and Corkum P B 2014 *Phys. Rev. Lett.* **113** 263005

[78] Chelkowski S, Bandrauk A and Corkum P B 2017 *Phys. Rev. A* **95** 053402

[79] He Pei-Lun, Lao Di and He Feng 2017 *Phys. Rev. Lett.* **118** 163203

[80] Wang M X, Xiao X R, Liang H, Chen S G and Peng L Y 2017 *Phys. Rev. A* **96** 043414

[81] Wang M X, Liang H, Xiao X R, Chen S G and Peng L Y 2019 *Phys. Rev. A* **99** 023407

[82] Smeenk C T L, Arissian L, Zhou B, Mysyrowicz A, Villeneuve D M, Staudte A and Corkum P B 2011 *Phys. Rev. Lett.* **106** 193002

[83] Titi A S and Drake G W F 2012 *Phys. Rev. A* **85** 041404

[84] Liu J, Xia Q Z, Tao J F and Fu L B 2013 *Phys. Rev. A* **87** 041403

[85] Reiss H R 2013 *J. Phys. B* **46** 175601

[86] Klaiber M, Yakaboylu E, Bauke H, Hatsagortsyan K Z and Keitel C H 2013 *Phys. Rev. Lett.* **110** 153004

[87] Yakaboylu E, Klaiber M, Bauke H, Hatsagortsyan K Z and Keitel C H 2013 *Phys. Rev. A* **88** 063421

[88] Ludwig A, Maurer J, Mayer B W, Phillips C R, Gallmann L and Keller U 2014 *Phys. Rev. Lett.* **113** 243001

[89] Cricchio D, Fiordilino E and Hatsagortsyan K Z 2015 *Phys. Rev. A* **92** 023408

[90] Ivanov I A 2015 *Phys. Rev. A* **91** 043410

[91] Chelkowski S, Brauk A and Corkum P B 2015 *Phys. Rev. A* **92** 051401

[92] Tao J F, Xia Q Z, Cai J, Fu L B and Liu J 2017 *Phys. Rev. A* **95** 011402

[93] Daněk J, Hatsagortsyan K Z and Keitel C H 2018 *Phys. Rev. A* **97** 063409

[94] Maurer J, Willenberg B, Daněk J, Mayer B W, Phillips C R, Gallmann L, Klaiber M, Hatsagortsyan K Z, Keitel C H and Keller U 2018 *Phys. Rev. A* **97** 013404

[95] Klaiber M, Hatsagortsyan K Z and Keitel C H 2018 *Phys. Rev. Lett.* **120** 013201

[96] Dörr M, Potvliege R M and Shakeshaft R 1990 *Phys. Rev. Lett.* **64** 2003

[97] Pont M and Gavrila M 1990 *Phys. Rev. Lett.* **65** 2362

[98] Su Q and Eberly J H 1990 *J. Opt. Soc. Am. B* **7** 564

[99] Kulander K C, Schafer K J and Krause J L 1991 *Phys. Rev. Lett.* **66** 2601

[100] de Boer M P, Hoogenraad J H, Vrijen R B, Noordam L D and Muller H G 1993 *Phys. Rev. Lett.* **71** 3263

[101] de Boer M P, Hoogenraad J H, Vrijen R B, Constantinescu R C, Noordam L D and Muller H G 1994 *Phys. Rev. A* **50** 4085

[102] Eberly J H and Kulander K C 1993 *Science* **262** 1229

[103] van Druten N J, Constantinescu R C, Schins J M, Nieuwenhuize H and Muller H G 1997 *Phys. Rev. A* **55** 622

[104] Gavrila M 2002 *J. Phys. B* **35** R147

[105] Askeland S, Sørngård S A, Pilskog I, Nepstad R and Førre M 2011 *Phys. Rev. A* **84** 033423

[106] Joachain C J, Kylstra N J and Potvliege R M 2011 *Atoms in Intense Laser Fields* (Cambridge University Press) pp. 1–549

[107] Sørngård S A, Askeland S, Nepstad R and Førre M 2011 *Phys. Rev. A* **83** 033414

[108] Liu H, Liu Y, Fu L, Xin G, Ye D, Liu J, He X T, Yang Y, Liu X, Deng Y, Wu C and Gong Q 2012 *Phys. Rev. Lett.* **109** 093001

[109] Toyota K, Tolstikhin O I, Morishita T and Watanabe S 2007 *Phys. Rev. A* **76** 043418
[110] Toyota K, Tolstikhin O I, Morishita T and Watanabe S 2008 *Phys. Rev. A* **78** 033432
[111] Demekhin Ph V and Cederbaum L S 2012 *Phys. Rev. Lett.* **108** 253001
[112] Demekhin Ph V and Cederbaum L S 2012 *Phys. Rev. A* **86** 063412
[113] Yu C, Fu N, Zhang G and Yao J 2013 *Phys. Rev. A* **87** 043405
[114] Toyota K, Saalmann U and Rost J M 2015 *New J. Phys.* **17** 073005
[115] Toyota K 2016 *Phys. Rev. A* **94** 043411
[116] Artemyev A N, Müller A D, Hochstuhl D, Cederbaum L S and Demekhin Ph V 2016 *Phys. Rev. A* **93** 043418
[117] Baghery M, Saalmann U and Rost J M 2017 *Phys. Rev. Lett.* **118** 143202
[118] Ning Q C, Saalmann U and Rost J M 2018 *Phys. Rev. Lett.* **120** 033203
[119] Jiang W C and Burgdörfer J 2018 *Opt. Express* **26** 19921
[120] Wang M X, Liang H, Xiao X R, Chen S G, Jiang W C and Peng L Y 2018 *Phys. Rev. A* **98** 023412
[121] Dondera M, Muller H G and Gavrila M 2002 *Phys. Rev. A* **65** 031405
[122] Førre M, Selstø S, Hansen J P and Madsen L B 2005 *Phys. Rev. Lett.* **95** 043601
[123] Emelin M Y and Ryabikin M Y 2014 *Phys. Rev. A* **89** 013418
[124] Simonsen A S and Førre M 2015 *Phys. Rev. A* **92** 013405
[125] Keitel C H 2001 *Contemp. Phys.* **42** 353
[126] Hu S X and Keitel C H 2001 *Phys. Rev. A* **63** 053402
[127] Salamin Y, Hu S, Hatsagortsyan K and Keitel C 2006 *Phys. Rep.* **427** 41
[128] Yu X and Liu Y 2019 *Phys. Rev. A* **99** 053406
[129] Brennecke S and Lein M 2018 *J. Phys. B* **51** 094005
[130] Brennecke S and Lein M 2018 *Phys. Rev. A* **98** 063414
[131] McPherson A, Gibson G, Jara H, Johann U, Luk T S, McIntyre I A, Boyer K and Rhodes C K 1987 *J. Opt. Soc. Am.* **4** 595
[132] Ferray M, L'Huillier A, Li X F, Lompre L A, Mainfray G and Manus C 1988 *J. Phys. B* **21** L31
[133] Eden J 2004 *Prog. Quantum Electron.* **28** 197
[134] Xiong W H, Peng L Y and Gong Q 2017 *J. Phys. B* **50** 032001
[135] Zhao J and Zhao Z X 2010 *Chin. Phys. Lett.* **27** 063301
[136] Zhu X S, Zhang Q B, Lan P F and Lu P X 2016 *Acta Phys. Sin.* **65** 224207 (in Chinese)
[137] Zhong S Y, He X K, Teng H, Ye P, Wang L F, He P and Wei Z Y 2016 *Chin. Phys. B* **25** 023301
[138] Walser M W, Keitel C H, Scrinzi A and Brabec T 2000 *Phys. Rev. Lett.* **85** 5082
[139] Milošević D B, Hu S and Becker W 2000 *Phys. Rev. A* **63** 011403
[140] Kylstra N J, Potvliege R M and Joachain C J 2001 *J. Phys. B* **34** L55
[141] Milošević D B, Hu S X and Becker W 2002 *Laser Phys.* **12** 389
[142] Joachain C J, Kylstra N J and Potvliege R M 2003 *J. Mod. Opt.* **50** 313
[143] Emelin M Y and Ryabikin M Y 2013 *Quantum Electron.* **43** 211
[144] Zhu X and Wang Z 2016 *Opt. Commun.* **365** 125
[145] Pisanty E, Hickstein D D, Galloway B R, Durfee C G, Kapteyn H C, Murnane M M and Ivanov M 2018 *New J. Phys.* **20** 053036
[146] de Aldana J R V and Roso L 2002 *J. Phys. B* **35** 1633
[147] Bandrauk A D and Lu H Z 2006 *Phys. Rev. A* **73** 013412
[148] Mishra R, Kalita D J and Gupta A K 2012 *Eur. Phys. J. D* **66** 169
[149] Potvliege R M, Kylstra N J and Joachain C J 2000 *J. Phys. B* **33** L743
[150] Chirilă C C, Kylstra N J, Potvliege R M and Joachain C J 2002 *Phys. Rev. A* **66** 063411
[151] Bechler A and Pratt R H 1999 *J. Phys. B* **32** 2889
[152] Khalil T, Schmidtke B, Drescher M, Müller N and Heinzmann U 2002 *Phys. Rev. Lett.* **89** 053001
[153] Cherepkov N A and Semenov S K 2001 *J. Phys. B* **34** L495
[154] Cherepkov N A and Semenov S K 2001 *J. Phys. B* **34** L211
[155] Cherepkov N A, Semenov S K, Drescher M and Heinzmann U 2003 *J. Phys. B* **36** 3063
[156] Cormier E and Lambropoulos P 1996 *J. Phys. B* **29** 1667
[157] Førre M and Simonsen A S 2014 *Phys. Rev. A* **90** 053411
[158] Ivanov I A, Dubau J and Kim K T 2016 *Phys. Rev. A* **94** 033405
[159] Selstø S and Førre M 2007 *Phys. Rev. A* **76** 023427
[160] Førre M and Simonsen A S 2016 *Phys. Rev. A* **93** 013423
[161] Lindblom T K, Førre M, Lindroth E and Selstø S 2018 *Phys. Rev. Lett.* **121** 253202
[162] Henneberger W C 1968 *Phys. Rev. Lett.* **21** 838
[163] Power E A and Zienau S 1959 *Philos. Trans. R. Soc. London, Ser. A* **251** 427
[164] Woolley R G 1971 *Proc. Roy. Soc. Lond. A* **321** 557
[165] Liang H, Wang M X, Xiao X R, Gong Q and Peng L Y 2018 *Phys. Rev. A* **98** 063413
[166] Anzaki R, Shinohara Y, Sato T and Ishikawa K L 2018 *Phys. Rev. A* **98** 063410
[167] Starace A F 1982 *Theory of Atomic Photonionization* in Handbuch der Physik (Springer, Berlin: Mehlhorn W) pp. 1–121
[168] Pronin E A, Starace A F, Frolov M V and Manakov N L 2009 *Phys. Rev. A* **80** 063403
[169] Pronin E A, Starace A F and Peng L Y 2011 *Phys. Rev. A* **84** 013417
[170] Cohen-Tannoudji C, Dupont-Roc J and Grynberg G 1998 *Atom–Photon Interactions* (John Wiley and Sons) pp. 1–656
[171] Maquet A, Véniard V and Marian T A 1998 *J. Phys. B* **31** 3743
[172] Krylovetsky A A, Manakov N L and Marmo S I 2001 *JETP* **92** 37
[173] Hu B, Liu J and Chen S G 1997 *Phys. Lett. A* **236** 533
[174] Xiao X R, Wang M X, Li M, Geng J W, Liu Y Q and Peng L Y 2016 *Acta Phys. Sin.* **65** 220203 (in Chinese)
[175] Perelomov A M, Popov V S and Terent'ev M V 1966 *Zh. Eksp. Teor. Fiz.* **50** 1393
Perelomov A M, Popov V S and Terent'ev M V 1966 *Sov. Phys. -JETP* **23** 924 (Engl. transl.)
[176] Ammosov M V, Delone N B and Krainov V P 1986 *Zh. Eksp. Teor. Fiz.* **91** 2008
Ammosov M V, Delone N B and Krainov V P 1986 *Sov. Phys. -JETP* **64** 1191 (Engl. transl.)
[177] Liu J 2014 *Classical Trajectory Perspective of Atomic Ionization in Strong Laser Fields* (Springer, Berlin, Heidelberg) pp. 1–84
[178] Daněk J, Hatsagortsyan K Z and Keitel C H 2018 *Phys. Rev. A* **97** 063410
[179] Verschl M and Keitel C H 2005 *Laser Phys.* **15** 529
[180] Böning B, Paufler W and Fritzsche S 2019 *Phys. Rev. A* **99** 053404
[181] Peng L Y and Starace A F 2006 *J. Chem. Phys.* **125** 154311
[182] Peng L Y, Jiang W C, Geng J W, Xiong W H and Gong Q 2015 *Phys. Rep.* **575** 1
[183] Bauer D and Koval P 2006 *Comput. Phys. Commun.* **174** 396
[184] Park T J and Light J C 1986 *J. Chem. Phys.* **85** 5870
[185] Leforestier C, Bisseling R H, Cerjan C, Feit M D, Friesner R, Guldberg A, Hammerich A, Jolicard G, Karrlein W, Meyer H D, Lipkin N, Roncero O and Kosloff R 1991 *J. Comput. Phys.* **94** 59
[186] Banerjee T, Deshmukh P C and Manson S T 2007 *Phys. Rev. A* **75** 042701
[187] Deshmukh P C, Banerjee T, Varma H R, Hemmers O, Guillemin R, Rolles D, Wolska A, Yu S W, Lindle D W, Johnson W R and Manson S T 2008 *J. Phys. B* **41** 021002
[188] Istomin A Y, Starace A F, Manakov N L, Meremianin A V, Kheifets A S and Bray I 2005 *Phys. Rev. A* **72** 052708
[189] Grum-Grzhimailo A N, Gryzlova E V and Meyer M 2012 *J. Phys. B* **45** 215602
[190] Briggs J S and Schmidt V 2000 *J. Phys. B* **33** R1
[191] Avaldi L and Huetz A 2005 *J. Phys. B* **38** S861
[192] Istomin A Y, Manakov N L, Meremianin A V and Starace A F 2004 *Phys. Rev. Lett.* **92** 063002
[193] Istomin A Y, Manakov N L, Meremianin A V and Starace A F 2004 *Phys. Rev. A* **70** 010702
[194] Istomin A Y, Manakov N L, Meremianin A V and Starace A F 2005 *Phys. Rev. A* **71** 052702
[195] Istomin A Y, Starace A F, Manakov N L, Meremianin A V, Kheifets A S and Bray I 2006 *J. Phys. B* **39** L35
[196] Pindzola M S, Robicheaux F, Loch S D, Berengut J C, Colgan J, Foster M, Griffin D C, Balance C P, Badnell N R, Witthoeft M C, Schultz D R and Minami T 2007 *J. Phys.: Conf. Ser.* **88** 012012
[197] Emmanouilidou A and Meltzer T 2017 *Phys. Rev. A* **95** 033405
[198] Emmanouilidou A, Meltzer T and Corkum P B 2017 *J. Phys. B* **50** 225602
[199] Ludlow J A, Colgan J, Lee T G, Pindzola M S and Robicheaux F 2009 *J. Phys. B* **42** 225204
[200] Langhoff P W, Arce J C, Sheehy J A, Hemmers O, Wang H, Focke P, Sellin I A and Lindle D W 2001 *J. Electron Spectros. Relat. Phenomena* **114–116** 23

[201] Langhoff P W, Arce J C and Sheehy J A 2002 *J. Electron Spectros. Relat. Phenomena* **123** 117

[202] Dehmer J L and Dill D 1976 *J. Chem. Phys.* **65** 5327

[203] Cherepkov N A, Semenov S K, Hikosaka Y, Ito K, Motoki S and Yagishita A 2000 *Phys. Rev. Lett.* **84** 250

[204] Bolognesi P, Toffoli D, Decleva P, Feyer V, Pravica L and Avaldi L 2008 *J. Phys. B* **41** 221002

[205] Cohen H D and Fano U 1966 *Phys. Rev.* **150** 30

[206] Toffoli D, Stener M, Fronzoni G and Decleva P 2002 *Chem. Phys.* **276** 25

[207] Toffoli D and Decleva P 2008 *J. Chem. Phys.* **128** 234101

[208] Toffoli D and Decleva P 2010 *Phys. Rev. A* **81** 061201

[209] Lucchese R R, Montuoro R, Grum-Grzhimailo A N, Liu X J, Prümper G, Morishita Y, Saito N and Ueda K 2007 *J. Electron Spectros. Relat. Phenomena* **155** 95

[210] Brumboiu I E, Eriksson O and Norman P 2019 *J. Chem. Theor. Comput.* **15** 5483

[211] Baltenkov A S, Dolmatov V K, Manson S T and Msezane A Z 2004 *J. Phys. B* **37** 3837

[212] Lao D, He P L and He F 2016 *Phys. Rev. A* **93** 063403

[213] Amusia M Y, Drukarev E G, Gorshkov V G and Kazachkov M O 1975 *J. Phys. B* **8** 1248

[214] Drukarev E G and Mikhailov A I 2016 *Photoionization of Atoms in High-Energy Atomic Physics* (Springer, Cham) pp. 157–201

[215] Galstyan A G, Chuluunbaatar O, Popov Y V and Piraux B 2012 *Phys. Rev. A* **85** 023418

[216] Schöffler M S, Stuck C, Waitz M, Trinter F, Jahnke T, Lenz U, Jones M, Belkacem A, Landers A L, Pindzola M S, Cocke C L, Colgan J, Kheifets A, Bray I, Schmidt-Böcking H, Dörner R and Weber T 2013 *Phys. Rev. Lett.* **111** 013003

[217] Grundmann S, Trinter F, Bray A W, Eckart S, Rist J, Kastirke G, Metz D, Klumpp S, Viefhaus J, Schmidt L P H, Williams J B, Dörner R, Jahnke T, Schöffler M S and Kheifets A S 2018 *Phys. Rev. Lett.* **121** 173003

[218] Chen S G, Jiang W C, Grundmann S, Trinter F, Schöffler M S, Jahnke T, Dörner R, Liang H, Wang M X, Peng L Y and Gong Q 2019 *Phys. Rev. Lett.* submitted

[219] Koval P, Fritzsche S and Surzhykov A 2003 *J. Phys. B* **36** 873

[220] Koval P, Fritzsche S and Surzhykov A 2004 *J. Phys. B* **37** 375

[221] Varma H R, Ciappina M F, Rohringer N and Santra R 2009 *Phys. Rev. A* **80** 053424

[222] Bachau H, Dondera M and Florescu V 2014 *Phys. Rev. Lett.* **112** 073001

[223] Dondera M, Florescu V and Bachau H 2017 *Phys. Rev. A* **95** 023417

[224] Hofbrucker J, Volotka A V and Fritzsche S 2017 *Phys. Rev. A* **96** 013409

[225] Florescu V, Budriga O and Bachau H 2011 *Phys. Rev. A* **84** 033425

[226] Florescu V, Budriga O and Bachau H 2012 *Phys. Rev. A* **86** 033413

[227] Grum-Grzhimailo A N and Gryzlova E V 2014 *Phys. Rev. A* **89** 043424

[228] Peng L Y, Pronin E A and Starace A F 2008 *New J. Phys.* **10** 025030

[229] Hartung A, Eckart S, Brennecke S, Rist J, Trabert D, Fehre K, Richter M, Sann H, Zeller S, Henrichs K, Kastirke G, Hoehl J, Kalinin A, Schöffler M S, Jahnke T, Schmidt L P H, Lein M, Kunitski M and Dörner R 2019 *Nat. Phys.* s41567-019-0653-y

[230] Keil T and Bauer D 2017 *J. Phys. B* **50** 194002

[231] Daněk J, Klaiber M, Hatsagortsyan K Z, Keitel C H, Willenberg B, Maurer J, Mayer B W, Phillips C R, Gallmann L and Keller U 2018 *J. Phys. B* **51** 114001

[232] Willenberg B, Maurer J, Keller U, Daněk J, Klaiber M, Teeny N, Hatsagortsyan K Z and Keitel C H 2019 *Phys. Rev. A* **100** 033417

[233] Brennecke S and Lein M 2019 *Phys. Rev. A* **100** 033417

[234] Corkum P B 1993 *Phys. Rev. Lett.* **71** 1994

[235] Schafer K J, Yang B, DiMauro L F and Kulander K C 1993 *Phys. Rev. Lett.* **70** 1599

[236] Lewenstein M, Balcou P, Ivanov M Y, L'Huillier A and Corkum P B 1994 *Phys. Rev. A* **49** 2117

[237] Reiss H R 2000 *Phys. Rev. A* **63** 013409

[238] Palaniyappan S, Ghebregziabher I, DiChiara A, MacDonald J and Walker B C 2006 *Phys. Rev. A* **74** 033403

[239] Klaiber M, Hatsagortsyan K Z and Keitel C H 2007 *Phys. Rev. A* **75** 063413

[240] Hatsagortsyan K Z, Klaiber M, Müller C, Kohler M C and Keitel C H 2008 *J. Opt. Soc. Am. B* **25** B92

[241] Kohler M C, Pfeifer T, Hatsagortsyan K Z and Keitel C H 2012 *Adv. At. Mol. Opt. Phys.* **61** 159